Journal of Nuclear Medicine, published on February 3, 2022 as doi:10.2967/jnumed.121.263179

^{18}F-PFPN PET: a new and attractive imaging modality for patients with malignant melanoma

Running title: ^{18}F-PFPN imaging for malignant melanoma

Authors: Xiao Zhang[1,2,a], Mengting Li[1,2,a], Yongkang Gai[1,2], Jing Chen[3], Juan Tao[4], Liu Yang[4], Fan Hu[1,2], Wenyu Song[1,2], Tzu-Chen Yen[5,6], Xiaoli Lan[1,2]*

Affiliations:

[1] Department of Nuclear Medicine, Union Hospital, Tongji Medical College, Huazhong University of Science and Technology

[2] Hubei Key Laboratory of Molecular Imaging

[3] Cancer Center, Union Hospital, Tongji Medical College, Huazhong University of Science and Technology

[4] Department of Dermatology, Union Hospital, Tongji Medical College, Huazhong University of Science and Technology

[5] Department of Medicine and Molecular Imaging Center, Linkou Chang Gung Memorial Hospital and Chang Gung University

[6] APRINOIA Therapeutics Co., Ltd

[a] These authors contribute equally to this work.

*** Corresponding author**: Xiaoli Lan

Address: No. 1277 Jiefang Ave, Wuhan 430022, Hubei Province, China

Telephone/Fax number: 86-27-83692633

E-mail: LXL730724@hotmail.com

First author: Xiao Zhang

Address: No. 1277 Jiefang Ave, Wuhan 430022, Hubei Province, China

Telephone number: 86-13545394560

E-mail: zhangxiao199204@foxmail.com

Word count: 4999 words

Funding

This work was financially supported by National Natural Science Foundation of China (grants 81901783 and 82030052).

Authors' contributions

X. L.: study design; X. Z. and M. L.: manuscript writing; Y. G.: tracer synthesis and identification; J. C., J. T. and L. Y.: patient recruitment; W. S. and F. H.: image acquisition and interpretation; T. Y.: manuscript revision.

ABSTRACT

^{18}F-FDG PET has limited diagnostic applications in malignant melanoma (MM). ^{18}F-PFPN is a novel PET probe with high affinity and selectivity for melanin. We conducted a clinical study with two aims, firstly to investigate the biodistribution and radiation dosimetry of ^{18}F-PFPN in healthy volunteers, and secondly, to examine the diagnostic utility of ^{18}F-PFPN PET imaging in patients with MM. **Methods:** ^{18}F-PFPN was synthesized through a fluoro-for-tosyl exchange reaction. Five healthy volunteers were enrolled to investigate the biodistribution, pharmacokinetics, radiation dosimetry, and safety of the tracer. Subsequently, a total of 21 patients with clinically suspected or confirmed MM underwent both ^{18}F-PFPN PET/MR and ^{18}F-FDG PET/CT scans. Normalized maximum standardized uptake values of selected lesions were determined for both tracers and compared in patient- and lesion-based analyses. **Results:** ^{18}F-PFPN has elevated radiochemical yield and was highly stable *in vivo*. In healthy volunteers, ^{18}F-PFPN was safe and well-tolerated and its effective absorbed dose was comparable to that of ^{18}F-FDG. In patient-based analysis, ^{18}F-PFPN uptake was higher than ^{18}F-FDG for both primary tumors and nodal metastases. In lesion-based analysis,^{18}F-PFPN PET imaging could detect 365 metastases that were missed on ^{18}F-FDG PET. Additionally, ^{18}F-PFPN PET imaging had clinical value in distinguishing false-positive lesions on ^{18}F-FDG PET. **Conclusion:** ^{18}F-PFPN is a safe and well-tolerated melanin PET tracer. In a pilot clinical study, ^{18}F-PFPN PET imaging outperformed traditional ^{18}F-FDG PET in identifying both primary MM and its distant spread.

Keywords: ^{18}F-PFPN, ^{18}F-FDG, malignant melanoma, PET, diagnosis

Malignant melanoma (MM) is a highly aggressive tumor that poses a significant public health burden (*1*). The 5-year overall survival rates of patients with nodal and distant spread are as low as 65% and 25%, respectively. While early surgical excision of localized MM portends favorable outcomes (5-year overall survival: 98%). In this scenario, both prompt diagnosis and accurate disease staging are paramount to reduce mortality.

Traditional ^{18}F-FDG PET may be clinically useful for staging and therapeutic monitoring of advanced (stage III−IV) MM (*2*). However, the value of ^{18}F-FDG PET imaging in this malignancy is limited by the uptake in the liver and brain (*3*), which may ultimately compromise a reliable detection of primary or metastatic melanoma lesions in these anatomical sites. Additionally, ^{18}F-FDG PET does not have sufficient sensitivity to diagnose stage I−II MM (*4*) and is generally unable to identify small-sized (<1 cm) metastases to the lung, liver, and brain (*5*).

Recent advances in specific PET tracers, including MM-selective antibodies (*6,7*), α-melanocyte stimulating hormone receptor ligands (*5,8*), and peptides (*9,10*), have fostered our ability to identify MM lesions. Unfortunately, several caveats, including slow and limited tumor uptake, suboptimal *in vivo* stability, and elevated liver accumulation, still hamper their routine clinical application. One of the most promising molecular targets for the imaging of MM is melanin, which exists in most melanomas (>90%) (*11*). Several melanin-targeted radiopharmaceuticals, including ^{123}I-MEL008 (*12*), ^{18}F-FBZA (*13*), ^{18}F-MEL050 (*14*) and 4-^{11}C-MBZA (*15*), have been synthesized from benzamide, quinoxaline, or picolinamide and applied as PET and SPECT tracers. We have previously designed and synthesized a ^{18}F-labeled benzamide analogue as a melanin imaging tracer, termed ^{18}F-5-fluoro-N-(2-[diethylamino]ethyl)picolinamide (^{18}F-5-FPN). This probe characterized by high melanin affinity and favorable pharmacokinetic properties (*16,17*), has shown

promising preclinical value for the identification of small (< 2 mm in size) nodal and distant metastases from MM in mice (*18*). However, the relatively elevated hepatic tracer uptake of ^{18}F-5-FPN hindered its clinical applications. Subsequently, we optimized this probe to be a higher tumor-to-normal liver ratio and radiochemical yield, named ^{18}F-N-(2-diethylaminoethyl)-4-(2-[2-ethoxy]-ethoxy)pyridine (^{18}F-PFPN) (*19*).

To shed further light on the translational value of ^{18}F-PFPN as a melanin-targeted PET probe for MM imaging, we designed the current study with two principal aims. First, we sought to investigate the biodistribution and radiation dosimetry of ^{18}F-PFPN in healthy volunteers. Second, we examined, for the first time, the clinical utility of ^{18}F-PFPN PET imaging in patients with suspected or pathologically confirmed MM.

MATERIALS AND METHODS

Healthy Volunteers and Patients

The institutional review board approved this study and all subjects signed a written informed consent. Five healthy volunteers (3 women and 2 men; age range: 28–48 years; Supplemental Table. 1) were enrolled to investigate the biodistribution, pharmacokinetics, radiation dosimetry, and safety of ^{18}F-PFPN. Between 01/19/2021 and 06/19/2021, the patients with clinically suspected or confirmed MM were recruited. All patients underwent ^{18}F-FDG PET/CT and ^{18}F-PFPN PET/MR scans within one week. CT was performed when MRI was contraindicated (1 patient for metal implant). Patients with acute systemic diseases, electrolyte disorders, other known malignancies, aged less than 18 years, and pregnant or lactating women were then excluded.

Biodistribution and Radiation Dosimetry of ^{18}F-PFPN in Healthy Volunteers

^{18}F-PFPN was synthesized using the procedural steps outlined in Supplemental Fig. 1 (*19*). The procedures for determining the tracer biodistribution and the radiation dosimetry were described in Supplemental Fig. 2. In healthy volunteers, serial whole-body PET/MR scans were subsequently acquired on an integrated PET/MR scanner (SIGNA^{TM} PET/MR, GE Healthcare) at 30, 60, 120, and 240 min after tracer injection. At each time point, image acquisition was carried out immediately after biological specimens (blood and urine) collection. The tracer uptake in each major organ was determined by calculating the mean standardized uptake value (SUVmean). The pharmacokinetic profile of ^{18}F-PFPN was investigated by determining the radioactive count of blood, plasma samples and urine specimens collected at different time points using an automatic well-type gamma-counter (2470 Automatic Gamma Counter WIZARD; PerkinElmer). The radiation absorbed dose for each major organ was calculated using the OLINDA/EXM software, version 2.1. The healthy volunteers were asked to report any subjective abnormality within 1 h from the completion of the study procedures. Vital signs were determined in the pre-procedural phase and 4 h after tracer injection.

PET Imaging in Patients with Suspected or Pathologically Confirmed Malignant Melanoma

^{18}F-PFPN PET/MR images were acquired approximately 1 and 3 h after the intravenous injection of ^{18}F-PFPN (dose: 3.0–5.4 MBq/kg). ^{18}F-FDG PET/CT images were acquired approximately 60 min after the intravenous injection of ^{18}F-FDG (dose: 3.7–5.4 MBq/kg). All scans were from the brain to upper thigh (or the pelma when required).

Image Interpretation

Images were uploaded on an Advantage Workstation (version AW4.6, GE Healthcare) for registration, fusion, and interpretation. ^{18}F-PFPN and ^{18}F-FDG PET images were independently reviewed by two

experienced nuclear medicine physicians who were not blinded to patient clinical data and conventional imaging results. All discrepancies were resolved by consensus.

Regions of interest were drawn on transaxial slices, and raw maximum standardized uptake values (SUVmax) were automatically calculated to quantify ^{18}F-FDG and ^{18}F-PFPN uptake within each lesion. To improve the comparability of SUVmax values, raw data were normalized using the following formula:

$$Normalized\ SUVmax = Raw\ SUVmax / SUVbkgd.$$

where SUVbkgd indicates the mean SUV of the descending aorta.

Both patient- and lesion-based quantitative assessments were performed. Patient-based analysis included either the primary tumor or the single lesion showing the highest tracer uptake at each metastatic site. Lesion-based analysis for each site was carried out either on all lesions (when their count was equal to or less than 10) or the ten lesions that showed the highest tracer uptake (when their count was > 10). A visual scoring system was also applied and described in the supplement.

Statistical Analysis

Continuous variables are presented as means ± standard deviations. SUVmax values between groups were compared using the Student's *t*-test. Categorical variables were compared using the chi-square test. All analyses were undertaken in SPSS, version 22 (IBM, Armonk, NY, USA). Two-tailed *P* values <0.05 were considered statistically significant.

RESULTS

Quality Control and Radiochemistry of the ^{18}F-PFPN Tracer

^{18}F-PFPN was successfully synthesized. The radiochemical purity and specific activity of ^{18}F-PFPN

(*n*=5) was 97.38±1.99% and 101–165 GBq/mmol, respectively. This probe *in vivo* stability measured at 4 h post-injection was >95%. An illustrative high performance liquid chromatography image of the tracer in the urine is shown in Supplemental Fig. 3.

Biodistribution, Dosimetry, and Safety of ^{18}F-PFPN in Healthy Volunteers

For healthy volunteers, the ^{18}F-PFPN maximum intensity projection images are shown in Fig. 1. ^{18}F-PFPN uptake was visible in the renal pelvis and calices, ureters, gallbladder, urinary bladder, stomach, and the liver. Hepatic SUVmean values were found to decrease over time, being 4.51±0.75, 3.26±0.62, 2.45±0.40, and 1.74±0.28 at 30, 60, 120, and 240 min post-injection, respectively (Supplemental Fig. 4). A similar pattern was observed for blood uptake, which gradually decreased from $(2.65\pm0.20)\times10^{-3}$ % ID/g at 30 min post-injection to $(1.35\pm0.67)\times10^{-3}$ %ID/g at 240 min (Supplemental Fig. 5). Comparable results were evident for most organs, except the gallbladder, eyes, and urine. The tracer activity in the urine was 0.15±0.05%ID/g at 30 min post-injection and reached a peak value of 0.35±0.14%ID/g at 60 min, suggesting a rapid renal clearance. Concerning the eyes, we observed a SUVmean increase from 0.79±0.07 at 30 min post-injection to 1.32±0.30 at 240 min due to the presence of choroidal melanocytes and retinal pigment cells.

The estimated absorbed radiation dosimetry for different organs is depicted in Supplemental Table. 2. The urinary bladder wall showed the highest dose activity (1.73×10^{-1} mSv/MBq), followed by the kidneys. A mean absorbed dose of 7.37×10^{-3} mSv/MBq was observed in the eyes. The total effective dose was 2.01×10^{-2} mSv/MBq.

Neither immediate adverse reactions nor significant changes in vital signs were observed after tracer injection. Similarly, follow-up laboratory examinations did not reveal any abnormal changes in liver and kidney function tests.

Characteristics of Patients with Malignant Melanoma

A total of 21 patients (mean age: 54.86±11.58 years) with clinically suspected or confirmed MM were included in the study (Table 1). Nine patients underwent imaging for initial disease staging, whereas investigations in the remaining 12 were aimed at detecting recurrences. Most primary MMs were in the skin, followed by choroid membranes. One patient had an occult primary MM located in the rectum.

Comparison of ^{18}F-PFPN and ^{18}F-FDG PET Imaging in Patients with Malignant Melanoma

We subsequently compared ^{18}F-PFPN and ^{18}F-FDG PET imaging in MM patients (Table 2, Fig. 2). ^{18}F-PFPN PET could provide clear lesion delineation with an excellent contrast due to low background, especially in the brain and liver. On a patient-based analysis, both ^{18}F-PFPN and ^{18}F-FDG PET showed the same diagnostic performance (100%) for the detection of primary lesions; in addition, these two techniques performed similarly for identifying metastases (100.00% *versus* 94.44% in lymph nodes, 100.00% *versus* 87.50% in bone, 100.00% *versus* 71.43% in liver, 100.00% *versus* 66.67% in other sites, respectively). Significant differences were observed between SUVmax-^{18}F-PFPN and SUVmax-^{18}F-FDG values measured at 1 and 3 h for both primary lesions (P=0.022/0.008) and lymph node metastases (P=0.045/0.005), with the former tracer showing the higher uptake.

On a lesion-based analysis, ^{18}F-PFPN PET/MR detected a higher number of lesions compared with ^{18}F-FDG PET (365 additional lesions); the detection rates according to the anatomical distribution were as follows: lymph nodes (100.00% *versus* 79.03%, respectively), bone (100.00% *versus* 38.32%, respectively), liver (100.00% *versus* 34.75%, respectively) and other sites (100.00% *versus* 87.88%, respectively). The SUVmax-^{18}F-PFPN of the primary lesions, as well as of nodal, bone, and hepatic metastases significantly increased from 1 h to 3 h post-injection, respectively (P<0.05); conversely, a significant decrease was

observed for most tissues and organs. A similar increase in normalized SUVmax-^{18}F-PFPN was evident between 1 and 3 h. Notably, normalized SUVmax-^{18}F-PFPN values at 3 h were higher than SUVmax-^{18}F-FDG for most lesions (P<0.01). The original SUVmax data are shown in Supplemental Table. 3

On the visual scoring system (Fig. 3), ^{18}F-PFPN outperformed ^{18}F-FDG for the detection of distant metastases to the liver (10' *versus* 0'), bone (8' *versus* 0'), other distant sites (3' *versus* 0') and lymph nodes (8' *versus* 0'). The total scores for ^{18}F-PFPN and ^{18}F-FDG PET were 29' and 0', respectively.

Illustrative Case Reports

A 47-year-old man (patient #8, Fig. 4) underwent ^{18}F-PFPN PET for the detection of MM recurrences. ^{18}F-PFPN PET identified a higher number of lesions compared with ^{18}F-FDG PET (fold-change in lesion detection for ^{18}F-PFPN PET: 2-fold higher for nodal metastases, 3-fold higher for hepatic metastases, and 2.5-fold higher for bone metastases). Notably, ^{18}F-PFPN PET successfully detected lesions less than 2 mm.

In patient #16 (Fig. 5), high background activity caused by elevated physiologic tracer uptake in the brain prevented the identification of cerebral metastases on ^{18}F-FDG PET imaging; however, the lesions were clearly visible on ^{18}F-PFPN PET images. Besides, MR sequences provided diagnostic confirmation.

In patient #3 (Fig. 6), ^{18}F-PFPN PET, but not ^{18}F-FDG PET, correctly identified the primary lesion located in the left foot as an early-stage melanoma. Interestingly, cervical lymph nodes showed intense ^{18}F-FDG uptake, whereas the ^{18}F-PFPN accumulation was absent in these areas. The following-up results suggested to be inflammatory but not metastasis lesions and false-positive on ^{18}F-FDG PET.

Fig. 7 shows an illustrative case of ^{18}F-PFPN PET and ^{18}F-FDG PET findings in a woman with distant amelanotic lesions from MM. Melanoma cells unable to produce melanin were missed on ^{18}F-PFPN PET, which further confirmed the specificity of ^{18}F-PFPN as a melanin PET tracer.

DISCUSSION

There are two principal findings from this study. First, on analyzing the biodistribution, pharmacokinetics, radiation dosimetry, and safety of ^{18}F-PFPN in five healthy volunteers, we found that this melanin PET tracer was safe and well-tolerated; also, its radiation absorbed dose was comparable to ^{18}F-FDG. Second, in a pilot clinical investigation conducted in suspected or confirmed MM patients, ^{18}F-PFPN showed higher uptake than ^{18}F-FDG for both primary tumors and distant metastases. In a lesion-based analysis,^{18}F-PFPN PET imaging could detect 365 metastases that were missed on ^{18}F-FDG PET. Collectively, these data represent a promising step in understanding the clinical value of ^{18}F-PFPN PET imaging for diagnosing and detecting disease recurrences in MM.

While ^{18}F-FDG PET imaging has extensive applications in patients with solid malignancies (*20*), its clinical value in MM is beset by high false-positive rates (100% in early-stage MM) (*21*). In this scenario, there have been increasing efforts to develop novel PET tracers capable of recognizing and binding to melanin with high affinity and specificity. The melanin PET tracer used in this study (^{18}F-PFPN) was optimized and improved based on our previous nicotinamide probe ^{18}F-5-FPN (*17*). Compared with the parent molecule, ^{18}F-PFPN is characterized by a more favorable pharmacokinetic profile, importantly, the negligible hepatic accumulation and rapid renal clearance (*19*). Thus endow this tracer the capacity to be safely applied for clinical imaging studies.

However, a partial excretion may occur through the hepatobiliary system, which may at least in part account for both gallbladder and intestinal wall uptake. On another note, the annular tracer accumulation observed in the eyes can be explained by the presence of choroidal melanocytes and retinal pigment cells. In terms of radiation safety, the total effective dose of ^{18}F-PFPN was 0.020 mSv/MBq, which is comparable to

the whole-body effective dose of ^{18}F-FDG (0.019 mSv/MBq) (*22*). Collectively, these results prompted us to conduct the first clinical ^{18}F-PFPN PET imaging study in patients with MM.

First, on analyzing the diagnostic performances for the detection of primary MM, we found that ^{18}F-PFPN PET could identify early T-stage lesions (e.g., T2b). Additionally, significant differences were observed between SUVmax-^{18}F-PFPN and SUVmax-^{18}F-FDG values measured at 3 h for primary lesions – with the former tracer showing the highest uptake (3.92-fold higher than that of ^{18}F-FDG). Based on these findings, we subsequently examined the role of ^{18}F-PFPN PET imaging to identify distant metastases. While the results of ^{18}F-PFPN PET imaging led to modifications in disease staging for one patient only (1/9), this may be related to the high proportion of patients with advanced disease stages. Interestingly, ^{18}F-PFPN showed low background activity – ultimately allowing a reliable delineation of a higher number of distant lesions from MM – including those at nodal, bone, and hepatic sites. Pigmented lesions can appear hyperintense on T1WI MR images owing to the high number of negative melanin charges, which ultimately facilitate iron binding. In this scenario, the combination of ^{18}F-PFPN PET with MRI can increase image interpretation accuracy. Immune checkpoint inhibitions could enhance immune cells to kill tumors, which had been one of the main treatments for metastatic melanoma (*23*). ^{18}F-PFPN may provide an excellent possibility to distinguish between inflammatory processes and melanotic lesions through specific binding to melanin. Benefitting from this, ^{18}F-PFPN imaging could be a valuable tool to evaluate immune checkpoint inhibition efficacy by reflecting the changes of melanoma tumor cells. However, ^{18}F-PFPN PET may underperform traditional ^{18}F-FDG PET in less common amelanotic or hypomelanotic subtypes of MM, which comprise 2−8% of all cases. These lesions, whose appearance can mimic several benign and malignant conditions, continue to pose significant diagnostic challenges (*11*).

Our findings need to be interpreted in the context of some limitations. First, it would have been interesting to include patients with early-stage (I−II) MM; more research is necessary to confirm our findings and to evaluate the role of ^{18}F-PFPN PET imaging in this patient group. Second, our study focused on the clinical value of this imaging modality in patients with pigmented MM. One of the study patients had her distant amelanotic lesions missed on ^{18}F-PFPN PET; therefore, the possibility of non-pigmented lesions in patients with MM should be based on a comprehensively considering thorough clinical and imaging investigations. Finally, the single-center design may have limited the external validity of our results. Despite these limitations, our data represent a promising step in understanding the potential utility of ^{18}F-PFPN as a melanin tracer and may open new research directions. For example, labeling ^{18}F-PFPN with therapeutic radioisotopes may warrant further scrutiny as a potential therapeutic strategy in metastatic MM (*24*).

CONCLUSION

We conclude that ^{18}F-PFPN is a safe and well-tolerated melanin PET tracer. In a pilot clinical study, ^{18}F-PFPN PET imaging outperformed traditional ^{18}F-FDG PET in identifying both primary MM and distant metastases. Further research is needed to verify these results in a larger sample and investigate the clinical value of ^{18}F-PFPN PET imaging in early-stage MM.

DISCLOSURE

Tzu-Chen Yen is an employee of APRINOIA Therapeutics Co., Ltd. Other authors have no conflicts of interest.

ACKNOWLEGDMENTS

We thank Chunxia Qin for technical assistance.

KEY POINTS

QUESTION: ^{18}F-PFPN is a novel PET probe with high affinity and selectivity for melanin, it may have clinical utility in patients with malignant melanoma (MM).

PERTINENT FINDINGS: In MM patients, ^{18}F-PFPN uptake was higher than that of ^{18}F-FDG for both primary tumors and metastases, and ^{18}F-PFPN could detect 365 metastases missed on ^{18}F-FDG PET. Additionally, ^{18}F-PFPN PET had clinical value in distinguishing false-positive lesions on ^{18}F-FDG PET.

IMPLICATIONS FOR PATIENT CARE: ^{18}F-PFPN imaging may outperform traditional ^{18}F-FDG PET in identifying both primary melanoma and its distant spread.

REFERENCES

1. Siegel RL, Miller KD, Fuchs HE, Jemal A. Cancer statistics, 2021. *CA Cancer J Clin.* 2021;71:7-33.
2. Schule SC, Eigentler TK, Garbe C, la Fougere C, Nikolaou K, Pfannenberg C. Influence of (18)F-FDG PET/CT on therapy management in patients with stage III/IV malignant melanoma. *Eur J Nucl Med Mol Imaging.* 2016;43:482-488.
3. Stelter L, Evans MJ, Jungbluth AA, et al. Novel mechanistic insights into arginine deiminase pharmacology suggest 18F-FDG is Not suitable to evaluate clinical response in melanoma. *J Nucl Med.* 2012;53:281-286.
4. Wagner JD, Schauwecker D, Davidson D, et al. Inefficacy of F-18 fluorodeoxy-D-glucose-positron emission tomography scans for initial evaluation in early-stage cutaneous melanoma. *Cancer.* 2005;104:570-579.
5. Cheng Z, Zhang L, Graves E, et al. Small-animal PET of melanocortin 1 receptor expression using a 18F-labeled alpha-melanocyte-stimulating hormone analog. *J Nucl Med.* 2007;48:987-994.
6. Revskaya E, Jongco AM, Sellers RS, et al. Radioimmunotherapy of experimental human metastatic melanoma with melanin-binding antibodies and in combination with dacarbazine. *Clin Cancer Res.* 2009;15:2373-2379.
7. Jandl T, Revskaya E, Jiang Z, Bryan RA, Casadevall A, Dadachova E. Complement-dependent cytotoxicity of an antibody to melanin in radioimmunotherapy of metastatic melanoma. *Immunotherapy.* 2013;5:357-364.
8. Gao F, Sihver W, Jurischka C, et al. Radiopharmacological characterization of ^{64}Cu-labeled α-MSH analogs for potential use in imaging of malignant melanoma. *Amino Acids.* 2016;48:833-847.
9. Beaino W, Anderson CJ. PET imaging of very late antigen-4 in melanoma: comparison of ^{68}Ga- and ^{64}Cu-labeled NODAGA and CB-TE1A1P-LLP2A conjugates. *J Nucl Med.* 2014;55:1856-1863.
10. Wei W, Ehlerding EB, Lan X, Luo Q, Cai W. PET and SPECT imaging of melanoma: the state of the art. *Eur J Nucl Med Mol Imaging.* 2018;45:132-150.
11. Thomas NE, Kricker A, Waxweiler WT, et al. Comparison of clinicopathologic features and survival of histopathologically amelanotic and pigmented melanomas: a population-based study. *JAMA Dermatol.* 2014;150:1306-1314.
12. Liu X, Pham TQ, Berghofer P, et al. Synthesis and evaluation of novel radioiodinated nicotinamides for malignant melanoma. *Nucl Med Biol.* 2008;35:769-781.
13. Ma X, Wang S, Wang S, et al. Biodistribution, radiation dosimetry, and clinical application of a melanin-targeted PET probe, ^{18}F-P3BZA, in patients. *J Nucl Med.* 2019;60:16-22.
14. Rizzo-Padoin N, Chaussard M, Vignal N, et al. [^{18}F]MEL050 as a melanin-targeted PET tracer: Fully automated radiosynthesis and comparison to ^{18}F-FDG for the detection of pigmented melanoma in mice primary subcutaneous tumors and pulmonary metastases. *Nucl Med Biol.* 2016;43:773-780.
15. Garg PK, Nazih R, Wu Y, Singh R, Garg S. 4-^{11}C-methoxy *N*-(2-diethylaminoethyl) benzamide: a novel probe to selectively target melanoma. *J Nucl Med.* 2017;58:827-832.
16. Liu M, Wang Y, Li M, et al. Using tyrosinase as a tri-modality reporter gene to monitor transplanted

stem cells in acute myocardial infarction. *Exp Mol Med.* 2018;50:1-10.

17. Feng H, Xia X, Li C, et al. Imaging malignant melanoma with (18)F-5-FPN. *Eur J Nucl Med Mol Imaging.* 2016;43:113-122.
18. Wang Y, Li M, Zhang Y, et al. Detection of melanoma metastases with PET-comparison of ^{18}F-5-FPN with ^{18}F-FDG. *Nucl Med Biol.* 2017;50:33-38.
19. Xu X, Yuan L, Yin L, et al. Synthesis and preclinical evaluation of ^{18}F-PEG$_3$-FPN for the detection of metastatic pigmented melanoma. *Mol Pharm.* 2017;14:3896-3905.
20. Groheux D, Cochet A, Humbert O, Alberini JL, Hindié E, Mankoff D. ^{18}F-FDG PET/CT for staging andrestaging of breast cancer. *J Nucl Med.* 2016;57(Suppl 1):17s-26s.
21. Acland KM, Healy C, Calonje E, et al. Comparison of positron emission tomography scanning and sentinel node biopsy in the detection of micrometastases of primary cutaneous malignant melanoma. *J Clin Oncol.* 2001;19:2674-2678.
22. Liu T, Liu C, Zhang Z, et al. ^{64}Cu-PSMA-BCH: a new radiotracer for delayed PET imaging of prostate cancer. *Eur J Nucl Med Mol Imaging.* 2021;48:4508-4516.
23. Dummer R, Lebbé C, Atkinson V, et al. Combined PD-1, BRAF and MEK inhibition in advanced BRAF-mutant melanoma: safety run-in and biomarker cohorts of COMBI-i. *Nat Med.* 2020;26:1557-1563.
24. Xu X, Yuan L, Gai Y, et al. Targeted radiotherapy of pigmented melanoma with ^{131}I-5-IPN. *J Exp Clin Cancer Res.* 2018;37:306.

FIGURES

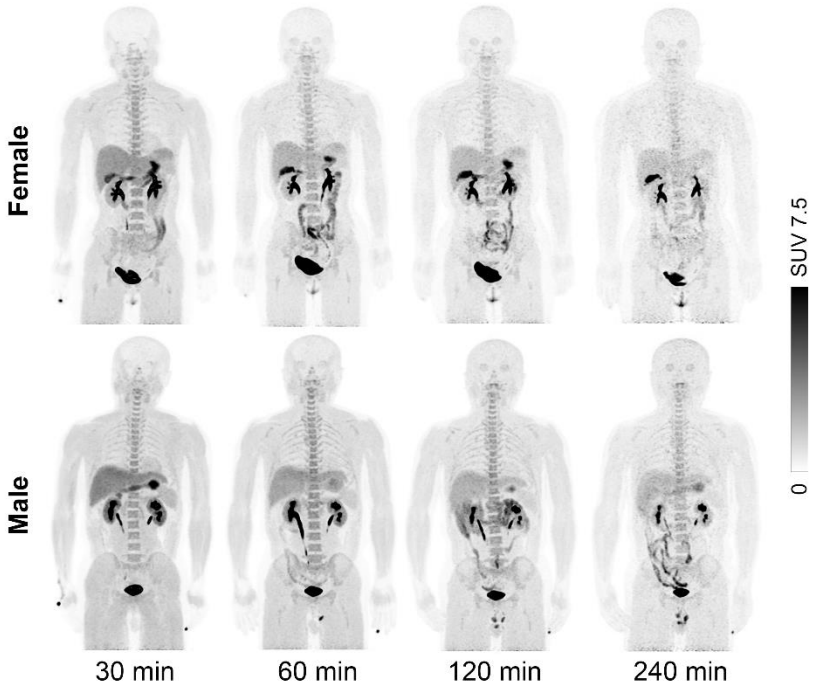

FIGURE 1. Maximum intensity projection (MIP) PET images obtained from female and male volunteers at different time points following intravenous ^{18}F-PFPN injection.

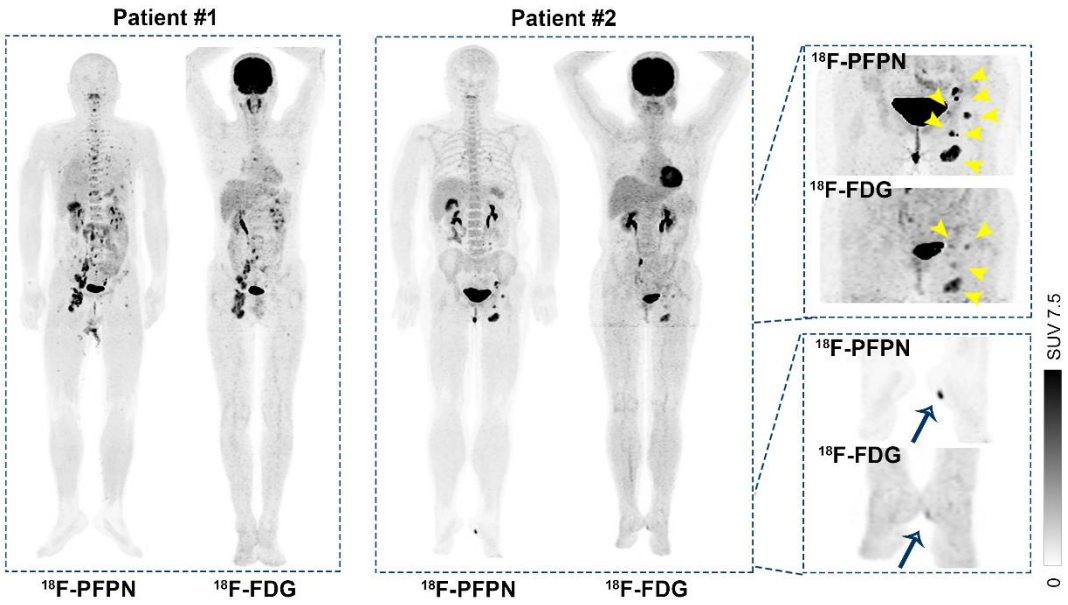

FIGURE 2. Representative images of patients with malignant melanoma (MM) who underwent ^{18}F-PFPN and ^{18}F-FDG PET scans for disease staging. ^{18}F-PFPN PET outperformed traditional ^{18}F-FDG PET for identifying both primary tumors and distant metastases. The blue arrows indicate the primary lesions, whereas yellow arrowheads denote lymph node metastases.

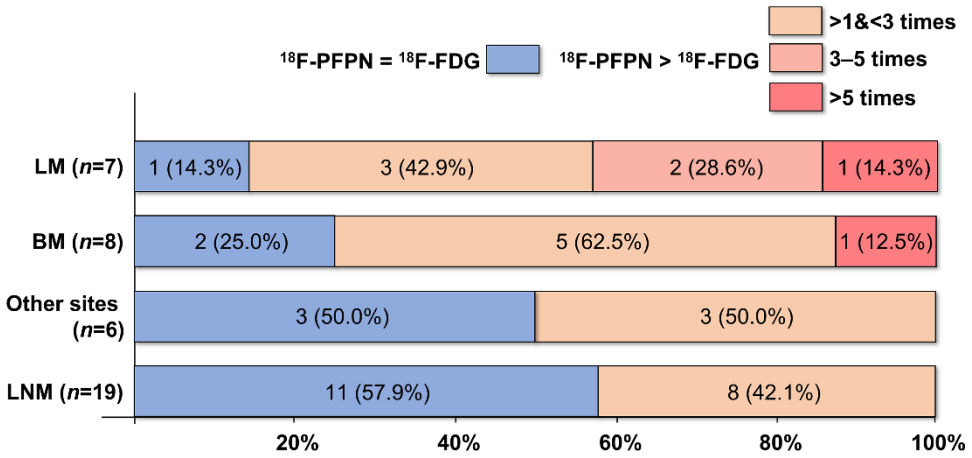

FIGURE 3. Comparative findings obtained from the visual assessment of ^{18}F-PFPN and ^{18}F-FDG PET images. Abbreviations: LM, liver metastases; BM, bone metastases; LNM, lymph node metastases.

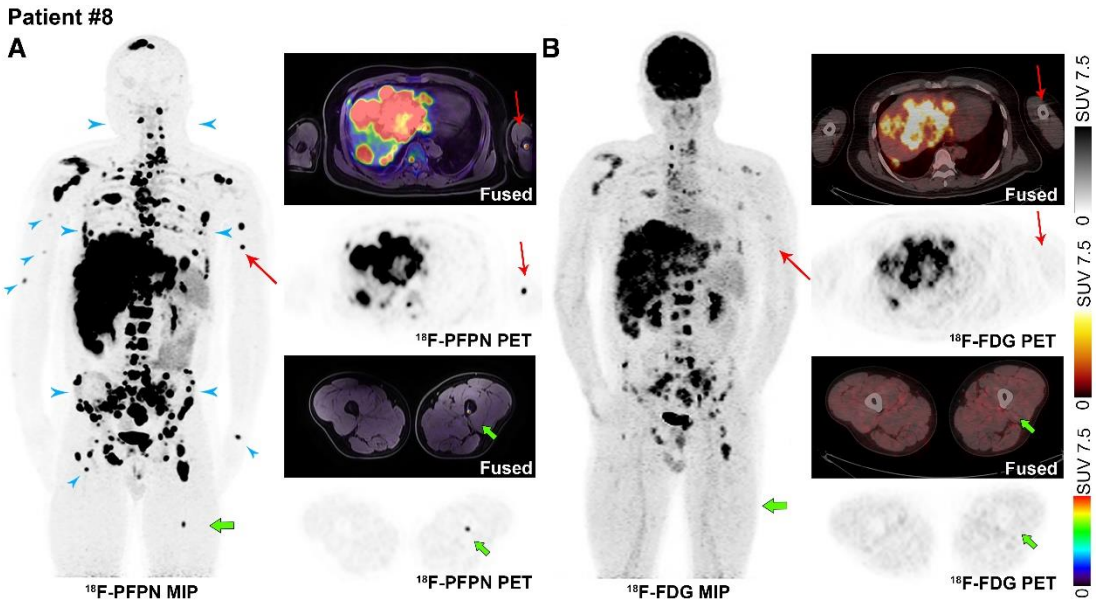

FIGURE 4. A 47-year-old man had undergone surgical removal of a choroidal MM 19 months before imaging. On MIP images, ^{18}F-PFPN PET (A) was able to identify a higher number of lesions (blue arrowheads) compared with ^{18}F-FDG PET (B). ^{18}F-PFPN PET/MR identified a hyper-intense T1WI focus of increased tracer uptake in the left arm (SUVmax: 8.4, red arrows) and left femur (SUVmax: 6.8, <2-mm, green arrows), which had normal uptake and density on ^{18}F-FDG PET/CT images.

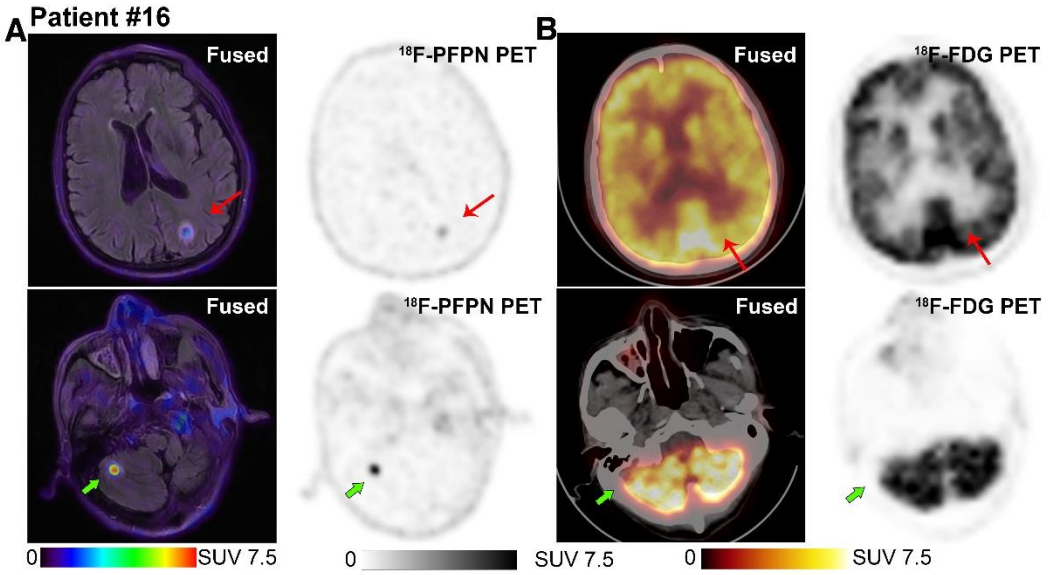

FIGURE 5. A 63-year-old man had undergone surgical removal of a plantar melanoma two years before PET imaging. Craniocerebral ^{18}F-PFPN PET/MR imaging (A) revealed avid tracer uptake in the left parietal lobe (SUVmax: 1.8, red arrows) and right cerebellum (SUVmax: 4.3, green arrows) Conversely, no malignant lesions were visible on ^{18}F-FDG PET; notably, these images were characterized by high background activity caused by elevated physiologic tracer uptake in the brain (B).

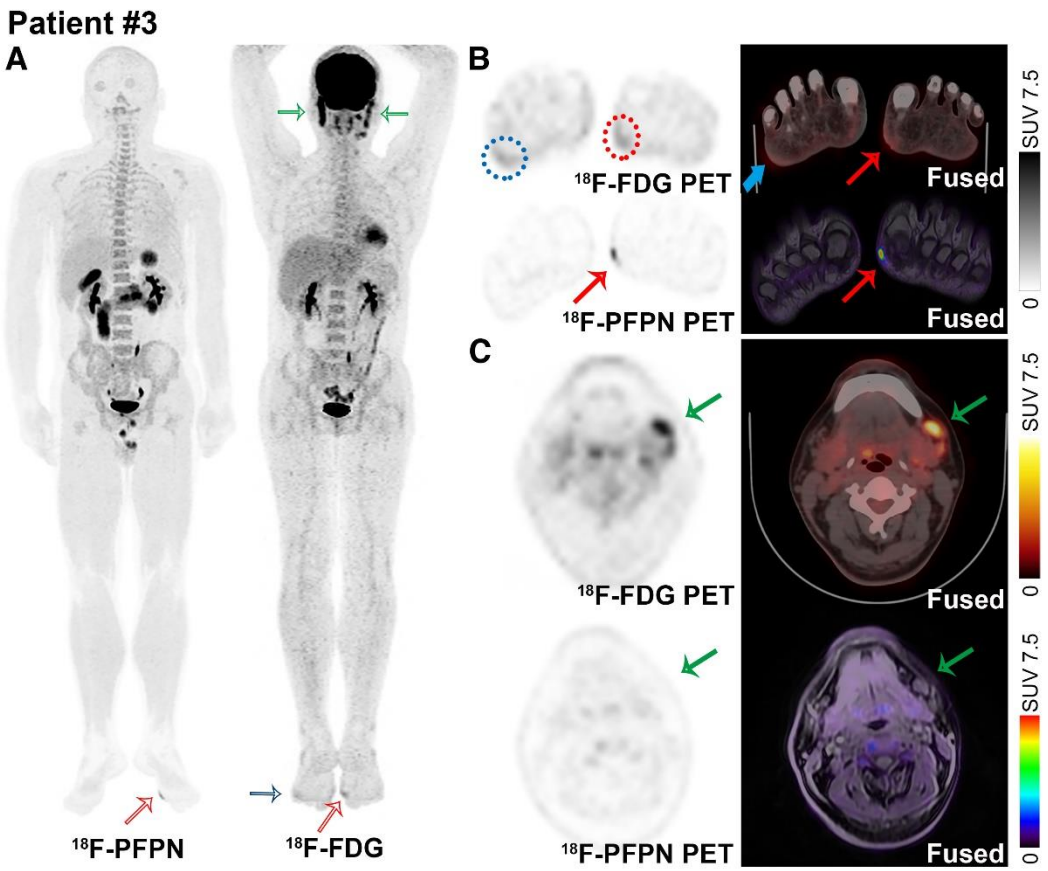

FIGURE 6. A 40-year-old man sought medical attention for a growing pigmented lesion located on the arch of the left foot. ^{18}F-FDG PET images (A and B) revealed mild tracer accumulations in the left anterior arch (red circle and red arrows; SUVmax: 3.3) and the lateral margin of the right foot (blue circle and blue arrows; SUVmax: 2.7). ^{18}F-PFPN PET was capable of providing a clear delineation of the lesion located in the left foot, which showed an avid tracer uptake (SUVmax: 5.0), but did not identify any lesion in the right foot. The results of pathology identified the left foot lesion as a nodular ulcerated MM (thickness: 1.2 mm; pathological T stage: pT2b). Interestingly, there was an intense ^{18}F-FDG uptake in the cervical lymph nodes (C, green arrows: SUVmax: 3.0–12.6) which, however, did not show significant ^{18}F-PFPN uptake. Collectively, these findings ruled out that these lesions were metastases from MM; ^{18}F-FDG PET-positive nodes likely had a reactive inflammatory nature.

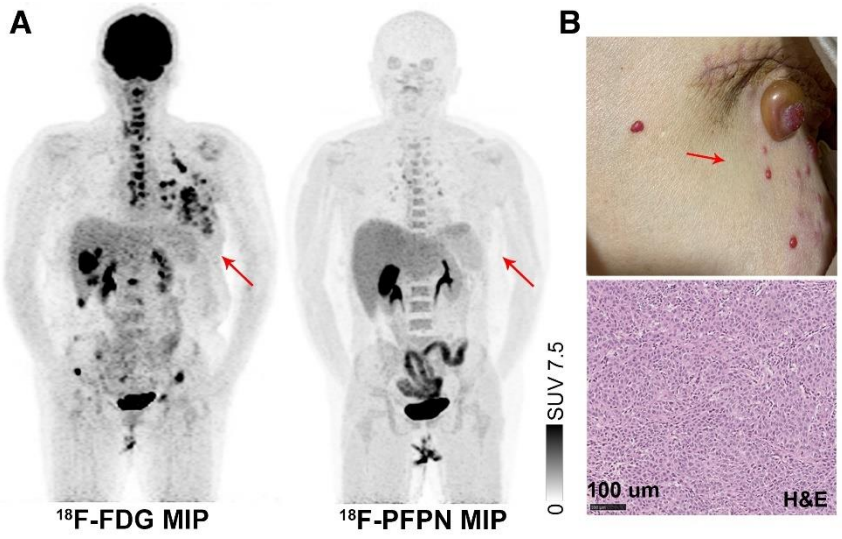

FIGURE 7. A 51-year-old woman had undergone partial excision of a malignant melanoma located in the left breast one year before PET imaging. She was regularly followed-up and a marked increase in serum CA 19-9 levels (>1200 U/mL, reference range: 0−35 U/mL) was evident over the last four months. On ^{18}F-FDG PET imaging, avid tracer uptake was evident in the operated breast (A, SUVmax: 3.7−10.4), axillary lymph nodes (SUVmax: 3.8−9.6), and the bone (SUVmax: 3.2−10.2), indicating recurrent disease. Unexpectedly, ^{18}F-PFPN PET imaging findings were negative. Visual examination of the operated breast showed that non-pigmented recurrent lesions (B). Pathology examination (hematoxylin and eosin staining) of axillary lymph nodes identified metastases from MM; however, these metastatic cells were proven to be non-pigmented (unable to produce melanin). Red arrows: breast lesion.

TABLES

TABLE 1. General characteristics of patients with clinically suspected or confirmed malignant melanoma

Patient number	Sex	Age (years)	Weight (Kg)	^{18}F-PFPN dose (MBq)	^{18}F-FDG dose (MBq)	Clinical role of PET	Primary tumor location	Confirmed metastases[a]	Clinical stage/final diagnosis
1	M	70	76	358.9	318.2	IS	Right plantar region	LNM, LM, BM, SM	T4bN3cM1, 4
2	F	55	54	270.1	244.2	IS	Left plantar region	LNM	T4bN3cM0, IIIc
3	M	40	73	344.1	314.5	IS	Left plantar region	-	T2bN0M0, IIa
4	M	47	55	214.6	259	RD	Occipital skin	LNM, GM	PD
5	M	67	59	196.1	266.4	IS	Right plantar region	LNM, LM, BM	T4bN3cM1, 4
6	M	59	69	266.4	281.2	RD	Left choroid (eye)	LM	PD
7	M	55	60	321.9	266.4	IS	Right plantar region	LNM, LM, BM	T4bN3cM1, 4
8	M	47	75	381.1	340.4	RD	Left choroid (eye)	LNM, LM, BM	PD
9	F	73	50	247.9	260.1	IS	Rectum	LNM, LM, BM, SM, PM	T4bN3cM1, 4
10	F	49	52	255.3	255.3	IS	Left isovarvas	LNM, BM	T3bN2bM1, 4
11	F	39	94	296	366.3	RD	Left pollex	LNM	PD
12	F	39	64	196.5	266.4	RD	Left plantar region	LNM	PD
13	F	63	60	303.4	273.8	RD	Right heel	LNM	PD
14	M	50	85	392.2	323.4	RD	Right plantar region	LNM, LM, BM, AM	PD
15	F	33	48	218.3	210.9	IS	Left arm	/	T4bN0M0, IIc
16	M	63	50	236.8	247.9	RD	Left heel	LNM, BM, PM, AM, CM, GM, CUM	PD
17	M	66	82	310.8	344.1	IS	Right forehead (skin)	LNM	T2aN2bM0, IIIb
18	F	54	60	247.9	259	RD	Perineum	LNM	PD
19	M	70	72	270.1	307.1	RD	Left plantar region	LNM	PD
20	F	50	67	270.1	254.2	RD	Left isovarvas	LNM, PM, CUM	PD
21	F	63	67	314.5	259	RD	Perineum	LNM	PD

Abbreviations: F, female; M, male; IS, initial staging; RD, recurrence detection; LNM, lymph node metastases; LM, liver metastases; BM, bone metastases; SM, spleen metastases; GM, gastric metastases; PM: pulmonary metastases; AM: adrenal gland metastasis; CM: cerebral metastasis; CUM: cutaneous metastasis; PD: progression of disease

[a]Confirmed after a thorough review of imaging and pathological findings.

TABLE 2. Patient- and lesion-based analyses of ^{18}F-PFPN and ^{18}F-FDG PET imaging findings

		Primary tumor	Lymph node metastases	Bone metastases	Liver metastases	Metastases to other sites
Patient-based analysis		8	18	8	7	6
Number of patients	^{18}F-FDG	8	17	7	5	6
	^{18}F-PFPN	8	18	8	7	6
	P value	/	1.0*	1.0*	0.462*	/
Normalized SUVmax	^{18}F-FDG	4.42±3.43	7.36±6.08	6.18±4.06	4.94±4.36	13.92±10.97
	^{18}F-PFPN 1 h	10.27±6.09	15.14±14.07	18.21±21.00	23.56±25.66	20.32±19.29
	^{18}F-PFPN 3 h	17.82±10.29	21.10±17.66	28.47±36.08	37.03±48.64	29.87±27.1
	P value (1/3 h)	0.022[a]/0.008[a]	0.043/0.005	0.161/0.130	0.144/0.178	0.496/0.211
Lesion-based analysis			124	394	141	33
Number of lesions	^{18}F-FDG		98	151	49	29
	^{18}F-PFPN		124	394	141	33
	P value		0.000	0.000	0.000	0.114[b]
Normalized SUVmax	^{18}F-FDG		5.36±4.08	5.01±2.33	5.08±2.11	7.93±7.70
	^{18}F-PFPN 1 h		10.88±9.49	20.14±21.83	19.17±17.29	11.97±11.59
	^{18}F-PFPN 3 h		16.35±13.55	31.83±37.09	31.55±31.52	17.52±16.56
	P value (1/3 h)		0.000/0.000	0.000/0.000	0.000/0.000	0.117/0.006

[a] Paired *t* test

[b] Fisher's exact test

P value (1/3 h) calculated for ^{18}F-FDG SUVmax *versus* ^{18}F-PFPN SUVmax at 1 or 3 h

Graphical Abstract

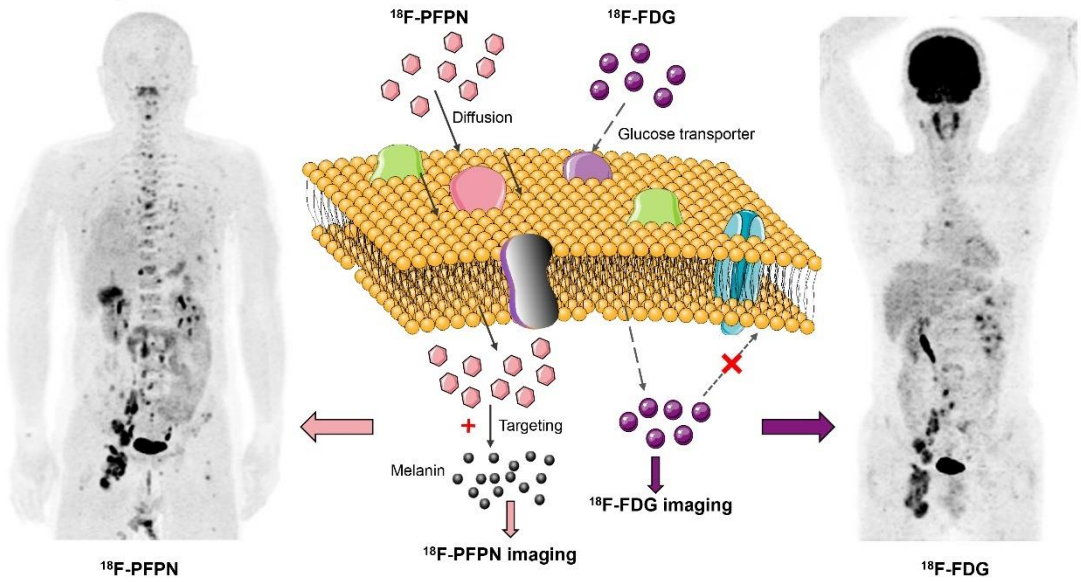

Supporting Information

Title: ^{18}F-PFPN PET: a new and attractive imaging modality for patients with malignant melanoma

Authors: Xiao Zhang[1,2,a], Mengting Li[1,2,a], Yongkang Gai[1,2], Jing Chen[3], Juan Tao[4], Liu Yang[4], Fan Hu[1,2], Wenyu Song[1,2], Qingyao Liu[1,2], Tzu-Chen Yen[5,6], Xiaoli Lan[1,2*]

The clinical study was approved by the institutional review board (approval number: 0016/2021) and registered at ClinicalTrials.gov (registration number: NCT04747561).

Table of Contents

Experimental Procedures----------Page 2−4

Results----------Page 5−9

Experimental Procedures

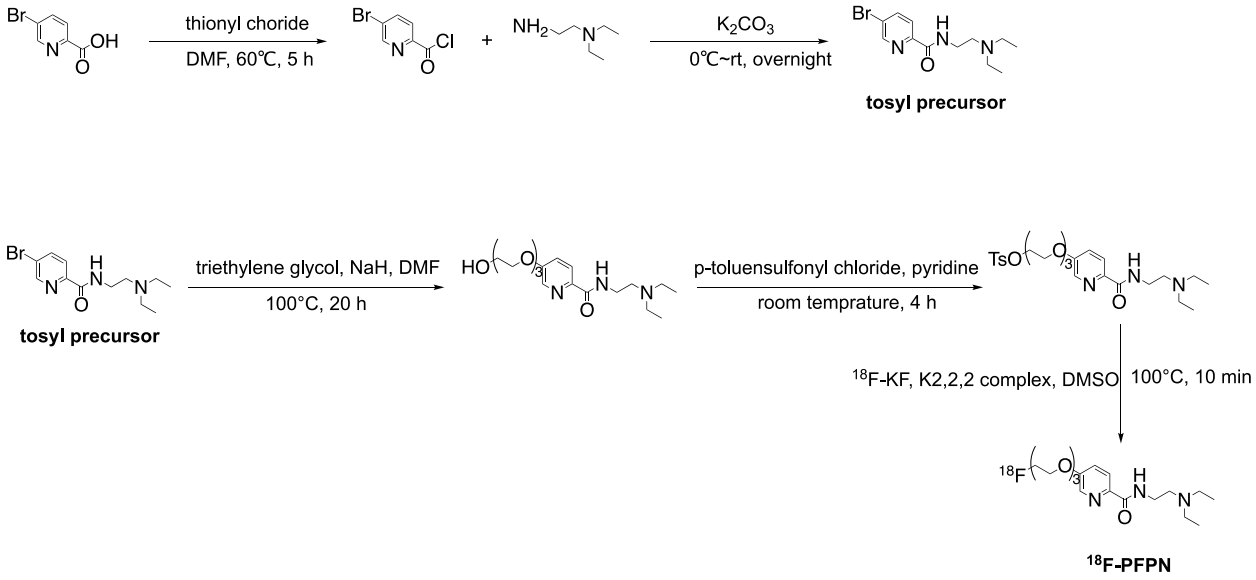

Using 5-bromo-N-2-pyridine-carboxylic acid as substrate, the tosyl precursor, 5-bromo-N-(2-(diethylamino)ethyl)picolinamide, was prepared through simple reaction and extraction. Subsequently, a triethylene glycol and p-toluensulfonyl chloride solution was added to the reaction system. The crude mixture was purified by silica gel chromatography to obtain toluene-4-sulfonicacid-2-(2-[2-{6-(2-diethylamino-ethylcarbamoyl)-pyridin-3-yloxy}-ethoxy]-ethoxy)-ethyl ester.

^{18}F-fluoride was produced through a ^{18}O (P, n) reaction in the GE tracer accelerator. All of the processes used for the radiochemical synthesis of ^{18}F-PFPN were undertaken on a GE Tracerlab FX_{FN} instrument using an automatic procedure. The aqueous [^{18}F] fluoride solution was transferred under nitrogen gas protection and subsequently retained in the activated quarternary methylamine (QMA) cartridge (Sep-Pak, Waters, Inc. Milford, MA, USA). Thereafter, ^{18}F was eluted into the reaction flask

with K_2CO_3 solution. Following the addition of the $K_{2,2,2}$ reagent, the solution was dried under a nitrogen flow. The precursor reagent solution was dissolved in anhydrous DMSO, added into the reaction flask, reacted at 100 °C for 10 min, and finally cooled down to 35 °C. The crude product was purified by HPLC and filtered through a 0.22-μm aseptic membrane filter for subsequent experiments.

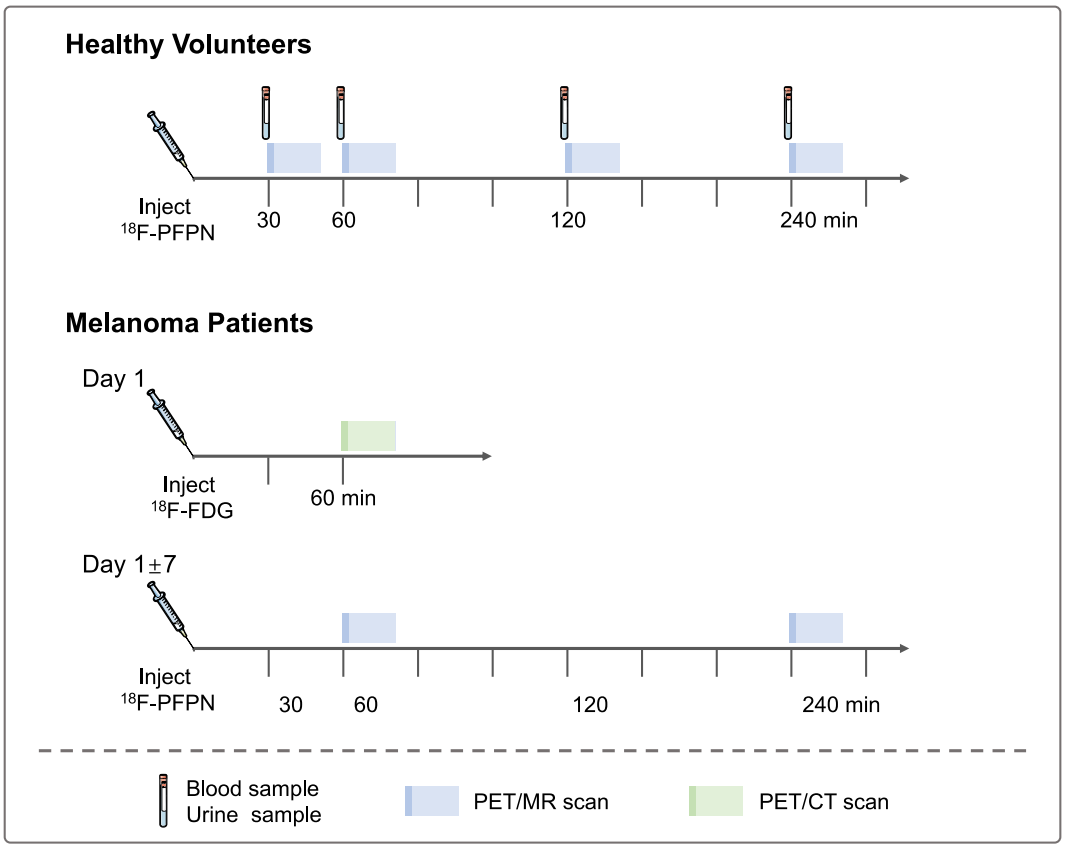

Supplemental Figure 2. Timelines for the dosimetry study in healthy volunteers (upper part) and the PET/CT and PET/MR imaging study in patients with malignant melanoma (lower part). Blood and urine samples were collected from healthy volunteers at 30, 60, 120, and 240 min after ^{18}F-PFPN injection; serial whole-body PET/MR scans were subsequently acquired. In patients with malignant melanoma, PET/MR imaging was performed approximately 1 h and 3 h after ^{18}F-PFPN injection. In addition, PET/CT images were acquired 1 h after ^{18}F-FDG intravenous injection.

Image Interpretation — a Visual Scoring System

A visual scoring system was subsequently devised to compare the clinical value of ^{18}F-PFPN and ^{18}F-FDG PET based on the number of lesions identified in each patient. When the number of lesions detected on ^{18}F-PFPN PET imaging outnumbered those identified on ^{18}F-FDG PET by 1–3, 3–5, and >5 folds, a score of 1', 2', and 3' was assigned to ^{18}F-PFPN PET imaging (and vice versa). A score of 0' means ^{18}F-PFPN PET and ^{18}F-FDG PET identified the same number of lesions. True or false positive lesions were confirmed after a thorough review of imaging, pathological findings or follow-up imaging examination.

RESULTS

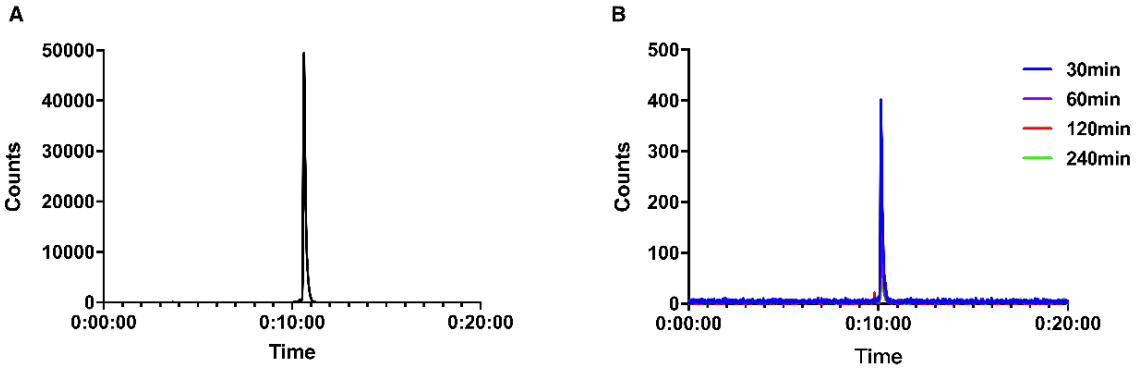

Supplemental Figure 3. (A) Radiochemical purity of ^{18}F-PFPN. (B) Stability of urinary ^{18}F-PFPN measured at different time points (30, 60, 120, and 240 min) after ^{18}F-PFPN injection.

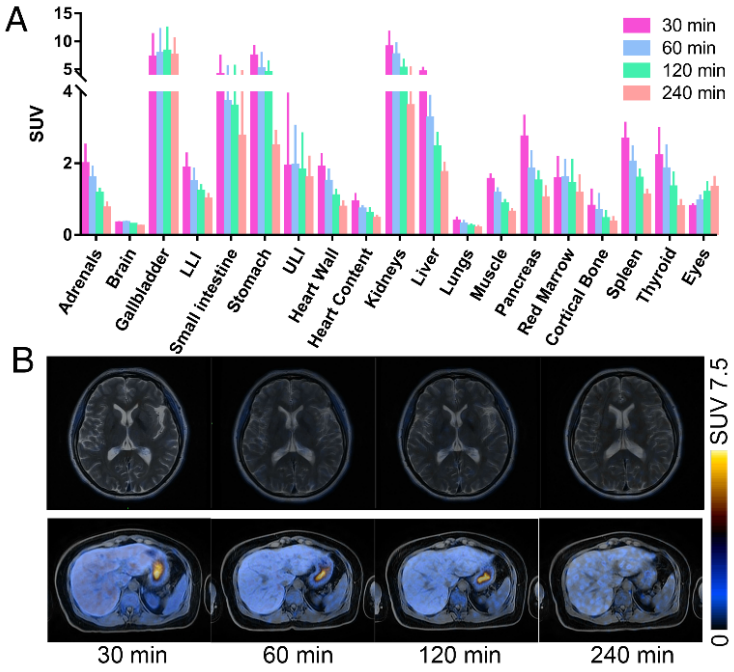

Supplemental Figure 4. SUVmean values of ^{18}F-PFPN uptake measured in various organs obtained from volunteers at different time points following intravenous ^{18}F-PFPN injection (A). The tomographic PET/MR images of the head and abdomen at different time points (B).

Tracer biodistribution in different biological matrices – including blood, plasma, and urine (Fig. S5). The uptake in blood and plasma gradually decreased from $(2.65 \pm 0.20)\times10^{-3}$ and $(2.67 \pm 0.28)\times10^{-3}$ % ID/g at 30 min post-injection to $(1.35 \pm 0.67)\times10^{-3}$ and $(1.38 \pm 0.47)\times10^{-3}$ %ID/g at 240 min post-injection, respectively (Fig. S5). Collectively, these findings indicate that ^{18}F-PFPN was rapidly cleared from the blood pool. The radioactivity in the urine reached its peak at 60 min (0.35 ± 0.14%ID/g) followed by a stepwise decrease.

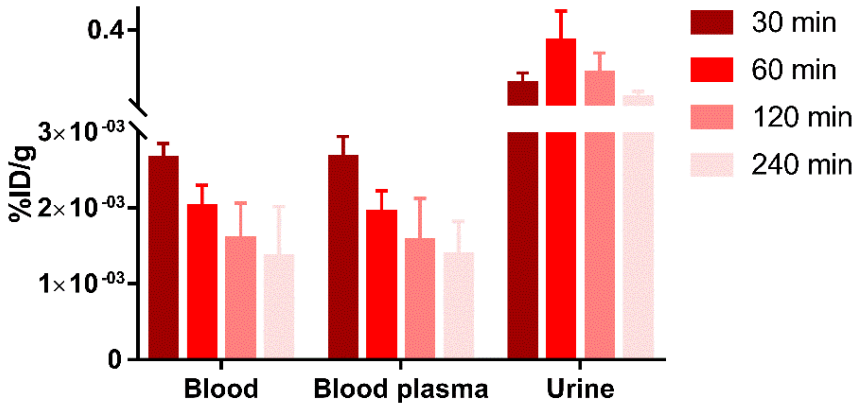

Supplemental Figure 5. The pharmaceutical kinetic of ^{18}F-PFPN in healthy volunteers.

Supplemental Table 1. General characteristics of the five healthy volunteers

Volunteer number	Sex	Age (years)	Weight (Kg)	Dosage (MBq)
1	F	48	58	185.0
2	F	29	55	188.7
3	F	28	65	225.7
4	M	30	71	181.3
5	M	38	66	199.8
Mean ± SD	-	34.60 ± 8.47	63.00 ± 6.44	196.10 ± 17.94

Abbreviations: F, female; M, male; SD: standard deviation

Supplemental Table 2. Estimated absorbed radiation dosimetry for ^{18}F-PFPN in different human organs

Organ	Dose (mSv/MBq)
Adrenals	2.26E-02
Brain	3.46E-03
Breasts (n = 3)	3.67E-03
Esophagus	9.65E-03
Eyes	7.37E-03
Gallbladder wall	4.12E-02
Left colon	1.22E-02
Small intestine	1.78E-02
Stomach wall	4.20E-02
Right colon	9.20E-03
Rectum	1.80E-02
Heart wall	1.32E-02
Kidneys	5.63E-02
Liver	3.11E-02
Lungs	5.26E-03
Ovaries (n = 3)	1.47E-02
Pancreas	2.36E-02
Salivary glands	1.09E-02
Red marrow	8.60E-03
Osteogenic cells	9.16E-03

Spleen	2.05E-02
Testes (n = 2)	1.05E-02
Thymus (n = 2)	6.10E-03
Thyroid	1.15E-02
Urinary bladder wall	1.73E-01
Uterus (n = 3)	2.86E-02
Total body	5.12E-03
Effective dose (mSv/MBq)	2.01E-02

The original values of ^{18}F-PFPN PET and ^{18}F-FDG PET were shown in Supplemental Table 3, which was the complement to Table 2. On a patient-based analysis, both ^{18}F-PFPN PET/MR and ^{18}F-FDG PET/CT showed similar diagnostic performance between original SUVmax-^{18}F-PFPN and SUVmax-^{18}F-FDG values for primary lesions and metastases. On a lesion-based analysis, original SUVmax-^{18}F-PFPN values were significantly higher than those of SUVmax-^{18}F-FDG for bone (both at 1 and 3 h) and hepatic metastases (at 3 h).

Supplemental Table 3. Original SUVmax of ^{18}F-PFPN PET and ^{18}F-FDG PET imaging findings

		Primary tumor	Lymph node metastases	Bone metastases	Liver metastases	Metastases to other sites
Patient-based analysis						
Original SUVmax	^{18}F-FDG	5.88±4.68	10.67±7.94	8.65±6.08	7.58±7.10	20.85±19.19
	^{18}F-PFPN 1 h	5.84±3.06	8.58±6.51	9.83±11.13	11.56±10.63	11.96±9.99
	^{18}F-PFPN 3 h	7.78±4.01	9.96±7.19	12.33±13.63	15.33±18.14	15.25±13.77
	P value (1/3 h)	0.980[a]/0.354[a]	0.399/0.783	0.807/0.523	0.485/0.391	0.338/0.574
Lesion-based analysis						
Original SUVmax	^{18}F-FDG		7.36±5.20	6.98±3.54	7.90±3.77	11.06±11.91
	^{18}F-PFPN 1 h		6.11±4.61	11.09±11.55	9.72±7.43	6.39±5.91
	^{18}F-PFPN 3 h		7.63±5.70	13.47±13.94	13.03±11.62	8.18±7.87
	P value (1/3 h)		0.116/0.760	0.017/0.002	0.209/0.019	0.051/0.261

[a] Paired *t* test

P value (1/3 h) calculated for ^{18}F-FDG SUVmax *versus* ^{18}F-PFPN SUVmax at 1 or 3 h